Three-dimensional electric-field vector measurement with an electro-optic sensing technique

Wen-Kai Kuo

Department of Electronics Engineering and Institute of Electronics, National Chiao Tung University and Precision Instrument Development Center, Taiwan

Yang-Tung Huang

Department of Electronics Engineering and Institute of Electronics, National Chiao Tung University, Taiwan

Sheng-Lung Huang

Institute of Electro-Optical Engineering, National Sun Yat-Sen University, Taiwan

Received July 7, 1999

A new technique for three-dimensional (3D) electric-field (e-field) vector measurement is presented. Three laser beams with different propagation paths in an electro-optic (EO) crystal were used to resolve 3D components of e-field vectors. We adopted a special geometric shape of bismuth silicon oxide EO crystal so that the three beams would propagate within it. A sensitivity of 0.6 V/cm $\sqrt{\text{Hz}}$ was achieved. A commercial Ansoft Maxwell 3D field simulator was also used to verify our measurements. © 1999 Optical Society of America

OCIS codes: 230.2090, 130.6010, 190.1900, 120.4290, 120.5410.

The external electro-optic (EO) probing technique has been proved to be an effective tool in characterizing electronic devices and circuits. It can be used to probe directly semiconductor devices and circuits on any substrate with pulsed[1] or continuous-wave[2] lasers. This approach also benefits from its noncontact and noninvasiveness properties for devices (or circuits) under test (DUT's). Recently this technique was used for near-field mapping of a radiation pattern above a microwave resonator.[3] In addition to field amplitudes, field-direction information is also very important for characterizing passive radio-frequency (rf) devices, such as chamfered bending transmission lines and patch antennas.[4] Another advantage of using the EO probing technique is that it can be extended to map two-dimensional (2D) electric-field (*e*-field) vectors on a circuit pattern and has been used to characterize a monolithic slot antenna.[5] However, in that study two kinds of EO material, $LiTaO_3$ and GaAs, were used to measure transverse and normal fields, respectively. Using different EO materials not only complicates measurement but also decreases accuracy because of the need for multiple calibrations. If *e*-field components along all axes can be obtained simultaneously, measurement and data analysis procedures can be greatly simplified. In the research reported in Ref. 6 a $LiTaO_3$ EO probe tip was used to measure 2D *e*-field vectors on a test pattern. However, $LiTaO_3$ is not suitable for three-dimensional (3D) measurement because the sensitivities for the three *e*-field components are not comparable with one another. In this Letter a bismuth silicon oxide [$Bi_{12}SiO_{20}$ (BSO)] EO crystal, which has excellent properties for measurement of 3D *e*-field vectors, is proposed to perform this characterization. The measured results are compared with simulation results obtained with a commercial Ansoft Maxwell 3D field simulator.

The EO probing technique is based on the linear EO effect, also known as the Pockels effect. In some crystals, applying an *e* field results in a change of polarization for an optical beam passing through the crystal. One can detect this change by combining an analyzer and photodetectors. The relationship between the applied *e* field and the polarization change can be described by an EO tensor. All EO crystals can be categorized into some symmetry groups. The symmetry group of $LiTaO_3$ is $3m$, and its EO tensor can be expressed as[7]

$$[r_{ij}] = \begin{bmatrix} 0 & -r_{22} & r_{13} \\ 0 & r_{22} & r_{13} \\ 0 & 0 & r_{33} \\ 0 & r_{51} & 0 \\ r_{51} & 0 & 0 \\ -r_{22} & 0 & 0 \end{bmatrix}. \tag{1}$$

Its corresponding index ellipsoid equation in the presence of a field $\mathbf{E} = (E_x, E_y, E_z)$ can be written as

$$x^2\left(\frac{1}{{n_o}^2} - r_{22}E_y + r_{13}E_z\right) + y^2\left(\frac{1}{{n_o}^2} + r_{22}E_y + r_{13}E_z\right) + z^2\left(\frac{1}{{n_e}^2} + r_{33}E_z\right) + 2r_{51}E_x yz + 2r_{51}E_y xz - 2r_{22}E_z xy = 1, \tag{2}$$

where $n_o = 2.176$ is the index of reflection when the polarization of the beam is along the x or the y direction and $n_e = 2.18$ is the index of reflection when the polarization of the beam is along the z direction without an e field, $r_{22} = -0.2$ pm/V, $r_{13} = 8.4$ pm/V, $r_{33} = 30.5$ pm/V, and $r_{51} = 22$ pm/V. It can be seen that the index values along three axes as a result of

0146-9592/99/221546-03$15.00/0

the EO deformation of the index ellipsoid are different and not comparable with one another. Therefore, analysis of the polarization changes of three individual components with $LiTaO_3$ by the EO probing technique is complicated. In addition, owing to the large differences among the tensor components, the sensitivities for different-bias e fields vary significantly. Consider another BSO EO crystal that has been used as a longitudinal probe tip.[8] Its symmetry group is 23, and its EO tensor is[7]

$$[r_{ij}] = \begin{bmatrix} 0 & 0 & 0 \\ 0 & 0 & 0 \\ 0 & 0 & 0 \\ r_{41} & 0 & 0 \\ 0 & r_{41} & 0 \\ 0 & 0 & r_{41} \end{bmatrix}. \tag{3}$$

The tensor's equation of the index ellipsoid in the presence of a field $\mathbf{E}$ is

$$\frac{x^2}{n^2} + \frac{y^2}{n^2} + \frac{z^2}{n^2} + 2r_{41}E_x yz + 2r_{41}E_y xz + 2r_{41}E_z xy = 1, \tag{4}$$

where $n = 2.54$ is the index of reflection when the polarization of the beam is along the x, y, or z direction without an e field and $r_{41} = 5.0$ pm/V. It can be seen that the three e-field components have the same effect on the EO deformation of the index ellipsoid for the BSO crystal, and thus the EO sensing technique with this BSO crystal has the same EO effect for three e-field components.

In our measurements of 3D e-field vectors three physically independent laser beams with different propagation paths inside the BSO EO prober (EOP) were employed. The geometric shape of the EOP and the propagation paths of the three laser beams are depicted in Fig. 1, in which the principal axes of this EO crystal are also indicated. The angles of incidence of beams 2 and 3 with respect to the bottom surface of the crystal are both 30°. As shown in the figure, the propagation path of beam 1 can be treated as though it lies along the y-axis direction of the crystal when its slanting angle from the normal of the EOP bottom plane is negligible. Then its polarization change is determined by the two principal axes of the following ellipse:

$$\frac{x^2}{n^2} + \frac{z^2}{n^2} + 2r_{41}E_y xz = 1. \tag{5}$$

Since the polarization change for beam 1 was affected mainly by the E_y component, that E_y component can be obtained by measurement of the polarization change. On the other hand, beams 2 and 3 propagated on the $x-y$ and $y-z$ planes of the EO crystal, respectively, so their polarization changes were affected not only by the E_y component but also by the E_x and the E_z components. Consequently, beam i ($i = 1$, 2, or 3), its EO retardation Φ_i of two eigenmodes, which causes the polarization change, can be expressed as

$$\Phi_i = k_{ix}E_x + k_{iy}E_y k_{iz}E_z. \tag{6}$$

All coefficients, k_{ix}, k_{iy}, and k_{iz}, can be calibrated by at least three known 3D e-field vectors, which can be obtained from simulations. Once all the coefficients are obtained and combined with the measured EO retardations, Φ_1, Φ_2, and Φ_3, of three beams, the three components of an unknown e-field vector $\mathbf{E}_u = (E_{xu}, E_{yu}, E_{zu})$ can be resolved by

$$\begin{pmatrix} E_{xu} \\ E_{yu} \\ E_{zu} \end{pmatrix} = \begin{bmatrix} k_{1x} & k_{1y} & k_{1z} \\ k_{2x} & k_{2y} & k_{2z} \\ k_{3x} & k_{3y} & k_{3z} \end{bmatrix}^{-1} \begin{pmatrix} \Phi_1 \\ \Phi_2 \\ \Phi_3 \end{pmatrix}. \tag{7}$$

Furthermore, the absolute calibration of the three e-field components requires that the EOP be put into a known standard e field. For some EO crystals it is possible to employ rotation of the polarization of a single probe beam to resolve two different e-field components if one of the components causes rotation of the principal axes and the other does not. However, this method is invalid for a BSO crystal because, according to Eq. (4), every e-field component causes the same 45° rotation of its corresponding principal axis. One cannot use two beams simultaneously to obtain three components either.

The experimental setup for our 3D e-field vector measurement is shown schematically in Fig. 2. The BSO EOP was glued onto fused silica for convenience of mounting on a cantilever beam. We polished the four inclined planes of the BSO EOP to reduce scattering loss. The thickness and the bottom area of the EOP were approximately 120 μm and 200 μm × 200 μm,

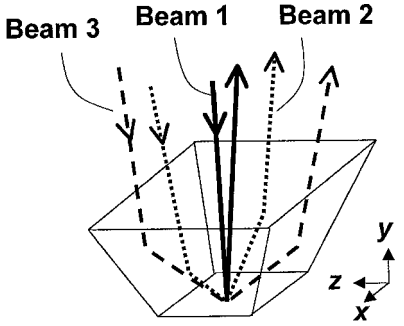

Fig. 1. Geometric shape of the EOP and the three laser beams. Beam 1 is along the y direction, beam 2 is on the $x-y$ plane, and beam 3 is on the $y-z$ plane.

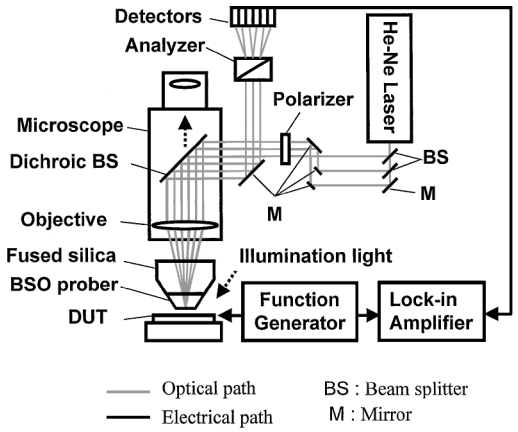

Fig. 2. Schematic illustration of the experimental setup for 3D e-field vector measurement.

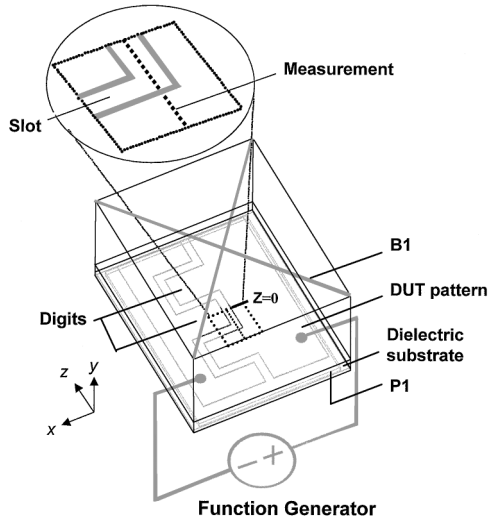

Fig. 3. DUT pattern and 3D simulation structure for the electromagnetic simulator. See text for definitions.

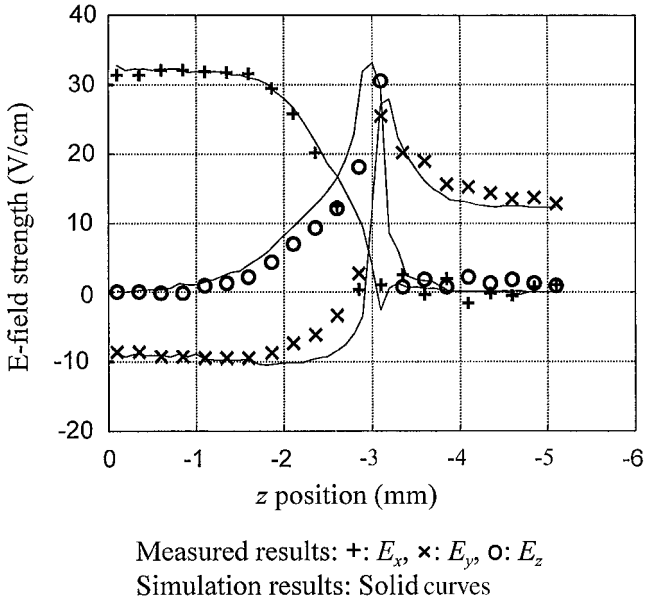

Fig. 4. Comparison between the measured and the simulation results.

respectively. The beam from a He–Ne laser head was split into three beams by two beam splitters and one mirror. All three beams passed a polarizer so that they would have the same linear polarization, which was parallel to the z axis of the principal axes of the EO crystal. Then the beams were redirected by a dichroic beam splitter. This beam splitter could let the illumination light pass; this light was reflected from the DUT. Then the three beams were focused with different paths inside the EOP by a 10× objective lens. After reflection from the bottom of the EOP, these three beams were picked off and fed into analyzers and detectors. The focusing positions of laser beams on the EOP could be observed from a viewing lens of the microscope. To improve the measurement sensitivity, we generated the test e field by use of a function generator to provide both a chopped dc signal for the DUT and a reference signal for the lock-in amplifier. For this experimental setup, a sensitivity of 0.6 V/cm $\sqrt{\text{Hz}}$ was achieved.

As shown in Fig. 3, our device structure for the experiment was an interdigital metal pattern on a dielectric substrate, which is generally used as a capacitance element in a rf circuit. The slot was 1 mm in width, and the digit was 4 mm in width. The most interesting area on this pattern is the corner of each digit. The EOP position was 30 μm above the metal pattern, and the e-field vectors were measured along the dashed line, which was located at the center of the slot, as indicated in Fig. 3. The distance between two measured points is 0.2 mm. Only one half of the whole line was measured because the other half-line could be obtained by symmetry. The 3D simulation structure with the electromagnetic simulator is also shown in Fig. 3. The metal plane, P1, below the dielectric was used to model the metallic stage for mounting of the DUT, and the boundary face, B1, on the top of the defined region was used to model the metallic structure of the microscope. A comparison between the measured and the simulation results is shown in Fig. 4. Good agreement was obtained for all three e-field components.

In summary, 3D e-field vector measurement by a BSO EO prober has been demonstrated successfully. Three different laser beams with different propagation paths were used to determine three individual components of the e-field vectors above the device under test. The measured results were in good agreement with the simulation results. With this technique, 3D e-field information can be obtained easily. This method is a very effective technique for characterizing and designing rf devices and circuits.

The authors thank the National Center for High-Performance Computing, National Science Council, Taiwan, for providing simulation hardware and software. They also thank Tom Kramer of the National Institute of Standards and Technology for his thoughtful correction of this paper. Y.-T. Huang's e-mail address is huangyt@cc.nctu.edu.tw.

References

1. M. S. Heutmaker and G. T. Harvey, Appl. Phys. Lett. **59,** 146 (1991).
2. D. L. Quang, D. Erasme, and B. Huyart, IEEE Trans. Microwave Theory Tech. **43,** 1031 (1995).
3. T. Pfeifer, T. Loffler, H. G. Roskos, H. Kurz, M. Singer, and E. M. Biebl, IEEE Trans. Antennas Propag. **46,** 284 (1998).
4. T. Ishii, *Microwave Engineering,* 2nd ed. (Harcourt Brace Jovanovitch, San Diego, Calif., 1989).
5. K. K. Kamoga, I. Toyoda, K. Nishikawa, and T. Tokumitsu, IEEE Microwave Guide Wave Lett. **4,** 414 (1994).
6. W. K. Kuo, S. L. Huang, T. S. Horng, and L. C. Chang, Opt. Commun. **149,** 55 (1998).
7. A. Yariv and P. Yeh, *Optical Waves in Crystal* (Wiley, New York, 1984).
8. R. Hofmann and H. J. Pfleiderer, Microelectron. Eng. **31,** 377 (1996).